Published in final edited form as:
J Phys Chem C Nanomater Interfaces. 2007 February 8; 111(5): 1955–1961. doi:10.1021/jp063996u.

Emission Behavior of Fluorescently Labeled Silver Nanoshell: Enhanced Self-Quenching by Metal Nanostructure

Jian Zhang, **Yi Fu**, and **Joseph R. Lakowicz***
Center for Fluorescence Spectroscopy, University of Maryland School of Medicine, Department of Biochemistry and Molecular Biology, 725 West Lombard Street, Baltimore, Maryland 21201

Abstract

Labeled silica beads with an *average* diameter of 100 nm were synthesized by incorporating with 20–600 μM $Ru(bpy)_3^{2+}$ complexes. Silver shells were deposited on the beads layer-by-layer with the shell thickness of 5–50 nm. The emission band became narrower and the intensity was enhanced depending on the shell thickness. Self-quenching of the probe was observed at high concentration. Poisson statistics were employed to analyze self-quenching of the fluorophores. The estimated quenching distance was extended from 6 to 16 nm with shell growth from 0 to 50 nm. Moreover, the silver shells were also labeled with Rhodamine 6G. Fluorescence enhancement and reduced lifetime were also observed for silver-silica shell containing R6G. We found that by adjustment of probe concentration and silver shell thickness, a $Ru(bpy)_3^{2+}$-labeled particle could be 600 times brighter than an isolated $Ru(bpy)_3^{2+}$ molecule. We expect labeled metal core–shell structures can become useful probes for high sensitivity and/or single particle assay.

Introduction

Recently more attention has been attracted to metallic nanoscale particles as the next generation superstructures in clinical diagnostic and biological detection.[1,2] How to develop sensitive detection techniques with these metal particles is of high interest. Fluorescence is widely utilized in biological sensing.[3] We now know that the fluorescence can be enhanced to (10–10^3)-fold by localizing a fluorophore near a metal nanoparticle, and the enhancement is suggested to occur via a coupling interaction of the fluorophore and the electric field around the metal particle, which can be induced by incident light or by the excited fluorophore.[4,5] The electric field derived from the metal particle is principally dependent on the cores such as metal, size, and shape, etc.,[6-8] which influence the coupling interaction with the fluorophore.

We are particularly concerned with the core/metal nanoshells.[9-11] It is thought that the electric fields in their cores are uniform according to theoretical calculations.[12,13] Fluorophores within the metal shells may thus be equally and efficiently enhanced if the cores are fluorescently labeled. Although there are many complexities arising when the fluorophores are placed very close to the metal surfaces, which depend to their chemical structures, orientations, and other unknown factors, some limited calculations are still available for spherical silver nanoshells.[11] The emission from a rhodamine dye is expected to be enhanced 10- to 100-fold when contained in a shell, which has been proven by our recent experimental results.[14a] Besides the emission enhancement, the shorter lifetimes of fluorophores in the metal shells result in less time for photochemistry while in the excited state, and thus more excitation–emission cycles prior to complete photobleaching.[4] The metal shells may also prevent the entrance of oxygen

*Address correspondence to this author. lakowicz@cfs.umbi.umd.edu..

and other species that react with the fluorophores and thus protect the fluorophores from photochemical reactions. These considerations indicate that metal shells containing fluorophores have a high potential as bright photostable probes.

In one of our recent publications, we have reported the synthesis and characterization of Ru(bpy)$_3^{2+}$-labeled silica beads. The beads were coated with silver shells, using layer-by-layer assembly to reach a shell thickness of 5–50 nm.[14a] The results revealed that the emission band from the Ru(bpy)$_3^{2+}$ complexes became narrower when emitting through the metal shells and the intensity was enhanced. Besides the shell thickness, the emission was also dependent on the size of silica cores. Lifetime measurements supported a coupling mechanism between the complex and the metal shell. However, we have not yet reported the correlation between emission properties and fluorophore concentration in the labeled shells, which is regarded as an important factor, in that context.

It is known that some fluorophores including the Ru(bpy)$_3^{2+}$ complex display a phenomena of self-quenching of the excited state especially at high concentration scale, and such quenching may occur via an energy transfer mechanism.[15] Our recent results reveal that Förster resonance energy transfer (FRET) between a donor and an acceptor can be enhanced as seen by an increase in the energy transfer rate and lengthening the Förster distance near a metal particle.[14b] Hence, we propose that the self-quenching between fluorophores in the metal shell has the opportunity to be enhanced. If this is true, then the fluorophores in metal shells are expected to behave differently from those in bare dielectric beads not coated with metal. An understanding of this effect will allow us to optimize the labeled shell and further develop bright plasmon-coupled probes (PCP). In this study, we still utilize the Ru(bpy)$_3^{2+}$ complex as a probe quantitatively incorporated silica bead with a certain size (diameter = 100 nm) because of its predictable quenching mechanism in the bead. The concentration ranged from 20 to 600 μM. The surfaces of the beads were aminated by using 3-aminopropyltrimethoxysilane then seeded by silver colloidal particles, and silver shells were deposited layer-by-layer up to a thickness of 50 nm.[9,10] The emission properties of Ru(bpy)$_3^{2+}$-labeled (Ru-labeled) metal shells were studied depending on the shell thickness at different probe concentrations. The effective distance for the self-quenching effect was analyzed by a Poisson statistical model.

We expect future PCPs to utilize the brightest available fluorophores. Hence we also studied rhodamine 6G (R6G) in silica bead coated with silver shell. R6G is known to aggregate progressively with a high concentration in silica gel.[16] In this work, R6G was also incorporated into the silica bead as an aggregated probe at high concentration, which is in a different state from the monomer of the Ru(bpy)$_3^{2+}$ complex. The silver shells were then deposited on the R6G-labeled silica. The emission properties were compared with those of Ru-labeled shells.

Experimental Section

All reagents and spectroscopic grade solvents were used as received from Fisher or Sigima/Aldrich. Nanopure water (>18.0 MΩ cm^2), purified using the Millipore Milli-Q gradient system, was used in all experiments.

1. Preparation of Dye-Labeled Silica Beads

Monodispersed silica beads were prepared with use of the Stöber method by co-dissolving Ru(bpy)$_3^{2+}$(ClO$_4$)$_2$ ranging from 2.0×10^{-7} to 6.0×10^{-6} M and tetraethyl orthosilicate (1.4×10^{-2} M) in 50 mL of ethanol. Ammonia alcohol solution (1.0 mL, 30%) was added dropwise under vigorous stirring (Scheme 1).[17] The solution became turbid after being stirred overnight due to the formation of silica beads. The mixture was centrifuged to remove the suspension, and the residual was washed thoroughly with ethanol. Combining the solutions, the concentration of Ru(bpy)$_3^{2+}$ in solution was measured quantitatively by the change of

fluorescence intensity. According to the differences between the initial and final fluorescence intensity in solutions, the local concentration of the complex in the beads was estimated. The beads were re-dispersed in 50 mL of ethanol and aminated by adding 10 μL of 3-aminopropyltrimethoxysilane with continuous stirring for 5 h. The aminated beads were centrifuged, washed with ethanol, and dispersed in 10 mL of water. The concentration of beads was estimated to be 6×10^{-8} M if the loss was neglected in the preparation and purification processes. R6G-labeled silica beads were synthesized by using the same protocol as that used for Ru-labeled beads in 1.0 μM R6G in solution.

2. Preparation of Metal Nanoshells

Silver colloids (*average* diameter = 20 nm) were prepared by reduction of silver nitrate (10 mM) with use of trisodium citrate (20 mM) in water at 95 °C.[1a] One milliliter of aminated silica beads suspension was added into 50 mL of silver colloidal solution with continuous stirring for 2 h to bind these silver colloids onto the silica beads. The supernatant was removed by centrifugation and the precipitate was redispersed in 10 mL of water. By using the colloid-bound silica beads as seeds, the silver shells were grown by reduction at 80 °C adding 1 mL of conjugate solution into 50 mL of $AgNO_3$ (10 mM) and sodium citrate (20 mM) water solution. The silver shells were recovered by centrifugation and then dispersed in water. The thick shells were grown layer-by-layer by repeating the above operations (Scheme 1). The solution amount of silver nitrate and sodium citrate was adjusted slightly in each operation to control the thickness of the silver shell.

3. Spectra Measurements

Absorption spectra were monitored with a Hewlett-Packard 8453 spectrophotometer. Fluorescence spectra were recorded with a Cary Eclipse fluorescence spectrophotometer. Lifetimes were measured by single photon counting, using a PicoQuant modular fluorescence lifetime spectrometer (Fluo Time 100) with PicoQuant 460–480 nm LED (LDH-P-L-470) as the light source. The collected data were analyzed with PicoQuant Fluofit 3.3 software. Transmission electron micrographs (TEM) were taken with a side-entry Philips electron microscope at 120 keV. Samples were cast from water solutions onto standard carbon-coated (200–300 Å) Formvar films on copper grids (200 mesh) by placing a droplet of a 1 mg/mL aqueous sample solution on grids. The size distribution of the metal cores was analyzed with Scion Image Beta Release 2 counting at least 200 particles.

Results and Discussion

1. Ru-Labeled Silver Shell

The formed silica beads were found to be uniform from the TEM images (Figure 1a). The average diameter was 100 nm,[10] independent of the existence of fluorophore in solution. The $Ru(bpy)_3^{2+}$ concentration in the silica beads, estimated by the difference of emission intensity in solutions before and after the bead formation, ranged from 2×10^{-5} to 60×10^{-5} M (Table 1).[18] According to the bead size, the concentration can be expressed as the number per bead (Table 1).

The silica bare beads do not display well-defined absorption spectra due to strong light scattering (not shown), but display emission spectra clearly with the maximal wavelength at 605 nm upon excitation at 450 nm, which is a 7 nm blue-shift from the free complex in water (Figure 2). Generally, the aggregation of fluorophores leads to a red-shift of the emission wavelength.[19] In this case, the wavelength is almost independent of the complex concentration in the bead, implying that the complexes mostly exist as monomers. The intensity is observed to increase proportionally with the concentration at the relatively low concentrations but displayed a downward derivation at high concentrations showing that the self-quenching occurs

(inset of Figure 2). A similar phenomenon is also observed by Ogawa in the mesoporous silica gel,[20] which is reported to be due to the self-quenching.

To prepare the silver-coated beads, we first made the silver colloids. The silver colloids with an average diameter of 15 nm were synthesized by reduction of silver nitrate with sodium citrate.[1] These small colloids were bound to the aminated beads to serve as the seeds (TEM images, Figure 1b) for a smooth growth of metal shells.[10c] The metal shells were first formed as islands on the silica beads (Figure 1c), and then became smooth when the seeding particles were covered by the metal shells after two cyclic treatments (Figure 1d). The shell became larger with an increase in the coating times (Figure 1d–f) representing a progressive shell growth. We followed the routine protocol from Halas in the coating operations,[9a] so it is believed that most particles should exist as the core–shell structures. Even though some solid colloidal particles were generated in solution, they were easily removed from the shells by centrifugation because of their smaller sizes (10–20 nm) and smaller mass. In any event, the solid silver colloidal particles cannot capture the probes and cannot contribute to the fluorescence measurements. The shell thickness was identified by subtracting the diameter of the silica bead from the total shell size. Each sample was counted from at least 50 TEM images, and the shell thicknesses were plotted as distributions (Figure 1g). Although the thickness is broaden-distributed, we still can determine that there is about 5 nm of shell growth per coating. Accordingly, the metal thickness of the first coating is defined to be 5 nm although a precise value is not available due to the irregular surface. When the metal thickness is over 50 nm, the shells become too heavy to be dispersed well in water.

The formation of metal shells can also be followed from the absorbance spectra. The silver colloids displayed a plasmon absorbance at 402 nm, but the shells display more intensive and broadened absorbance bands with shell growth. Simultaneously, the wavelength was red-shifted.[14a]

The emission spectra were collected upon excitation at 450 nm. The emission maximum near 610 nm does not alter with shell growth implying that the complex remains chemically intact in the silver shell. However, the emission band becomes significantly narrower with the shell growth to 20 nm (Figure 3a), consistent with our previous observation[14a] and the theoretical predication by Enderlein.[21] It is interesting to notice that the bandwidth is almost independent of the complex concentration in the shell, indicating that the narrowness is due to the metal shell. The emission intensity is strongly affected by the shell thickness, which initially increases and then decreases with the shell growth (inset of Figure 3a). The enhancement efficiency, estimated as a ratio of emission intensity from the shell over that of the bead at the same concentration, was observed to depend on the complex concentration in the shell. The measured values were plotted against the shell thickness (Figure 3b). It is noted that every series of sample at a certain concentration displays a maximal efficiency at a certain shell thickness and this value is shifted to thinner shells with increasing probe concentration.

2. R6G-Labeled Silver Shell

Silver shells were also deposited layer-by-layer on the R6G-labeled beads in an analogous protocol to the Ru-labeled shells. The concentration of R6G adsorbed in the silica bead was estimated to be 2×10^{-4} M, about twice of the concentration of adsorbed $Ru(bpy)_3^{2+}$ in the shell under the same conditions, indicating that R6G was adsorbed more strongly. The R6G-labeled shells displayed similar TEM images and absorbance spectra as the Ru-labeled shell.

The emission properties of R6G-labeled silica beads and silver shell particles were examined upon excitation at 500 nm. The emission maxima was at 571 nm (Figure 4), showing an obvious red-shif from that of free R6G in water (547 nm), but close to that of aggregated R6G in the silica gel.[16] We thus suggest that R6G mostly exist as aggregates in this case. The emission

wavelength does not alter with shell growth, implying that the R6G dimers are not influenced by the shell. It is noted that the emission band is not narrowed by the metal shell different from the Ru-labeled shell. The reason is uncertain, but may be due to the more narrow emission spectrum of R6G as compared to $Ru(bpy)_3^{2+}$ and thus a more uniform interaction with the metal over the R6B emission spectrum. This difference may also be due to the different chemical structures of R6G and $Ru(bpy)_3^{2+}$ that lead to their different interactions with the metal shells. We will solve this issue by fluorescently labeling metal shells with a range of fluorophores in future research. The emission intensity was observed to increase and then decrease with the shell growth (Figure 4). The enhancement efficiency was plotted against the shell thickness, showing a maximum for a 20 nm thick shell (inset of Figure 4). Because of the aggregation behavior of R6G in the silica particles it is a less favorable probe to study only fluorophore interactions with the shells.

3. Metal-Enhanced FRET for Ru-Labeled Silver Shell

From the concentration-dependent data, it is known that the maximal intensity of the particle occurs for a thinner shell with an increase in the complex concentration (Figure 3b). According to our observations of Surface Plasmon-Coupled Emission (SPCE), light can couple through the metal film into the far field.[22] Our results also indicate that the metal shells influence the interactions between the probes themselves. We propose that the emission from the metal shell particle depends on three factors: intensity enhancement, self-quenching enhancement, and quenching near the metal shell. The emission intensity (I_{app}) hence can be expressed as a sum of enhanced or plasmonic-coupled emission (I_{em}), nonradiative decay (I_{nr}), enhanced self-quenching (I_{sq}), and metal-quenching (I_{mq}) as eq 1. I_{em} contributes

$$I_{app}=I_{em}+I_{nr}+I_{sq}+I_{mq} \quad (1)$$

positively but I_{sq}, I_{mq}, and I_{nr} contribute negatively to the total intensity as the shells grow. Although I_{em} and I_{nr} can be estimated from theoretical stimulations, the treatment may be very complicated especially if the metal shells are not perfectly smooth. We found that the silver shell containing the lowest concentration (20 μM) displays an approximate linear intensity increase with the shell growth (Figure 3b), showing that the self-quenching is very weak. Utilizing the extended dash line from the thin silver shells as the theoretical reference (Figure 3b), the quenching fraction over the total was estimated from the differences between the reference and measured curves. The intensity at the same shell thickness is observed to rise at the beginning then decrease with an increase in the concentration (Figure 5).

We can set up a model to analyze the dependence of self-quenching on the shell thickness on the basis of the quenching. Assuming that an excited complex can be quenched completely when the nearest neighbor complex is localized within a certain distance, the distribution probability $P(r)$ of distance between the neighbor complexes in random distribution can be described simply in Poisson statistics as eq 2,[23]

$$P(r)=4\pi r^2 N_A\left(c\times 10^{-24}\right)\exp\left[-4\pi r^3 N_A\left(c\times 10^{-24}\right)/3\right] \quad (2)$$

where N_A is Avogadro's constant and c is the concentration of $Ru(bpy)_3^{2+}$ in the core. The distribution probability $P(r)$ is plotted against the distance between the complexes at different concentrations (Figure 6). The maximal probability is shifted to short distance, revealing that more complexes appear within a close distance, with an increase of concentration. By using the quenching fraction to fit this equation, the estimated distance is approximately regarded as the quenching distance. Subsequently, the quenching distances data are listed in Table 2 and

plotted against the shell thickness (Figure 7). The self-quenching distance was found to depend on shell thickness but to be almost independent of the probe concentration. The value is increased from 6 nm on the bare bead to 16 nm in the 50 nm thick shell, showing that the self-quenching distance is increased 170%. This enhancement is even higher than that obtained from a donor–acceptor pair near a metal particle (70%),[15] implying that the metal shells can enhance the energy transfer more efficiently in the interior electric field.

The R6G-labeled shells are not analyzed here because of lack of concentration-dependence data. In addition, the presence of monomers and aggregates of R6G make the analysis complicated. The enhancement at the concentration of 2×10^{-4} M displays a maximum at a shell thickness of 20 nm (Figure 4), indicating that the aggregated R6G can be quenched more efficiently than the monomer $Ru(bpy)_3^{2+}$ complex.

4. Intensity Decays

Lifetime is an important parameter to evaluate the interactions between the fluorophores and the metal plasmon resonance.[3] The fluorescence intensity decay curves were analyzed in terms of a sum of individual single-exponential decays:[24]

$$I(t) = \sum_{i=1}^{n} \alpha_i \exp(-t/\tau_i) \tag{3}$$

In this expression τ_i values are the decay times and α_i values are the amplitudes. The fractional contribution of each component to the steady-state intensity is described by:

$$f_i = \frac{\alpha_i \tau_i}{\sum_j \alpha_j \tau_j} \tag{4}$$

The average lifetime is represented by:

$$\bar{\tau} = \sum_i f_i \tau_i \tag{5}$$

The decay curves of Ru-labeled silica bead and silver shells were analyzed by a double-exponential model and parameters are listed in Table 3. The *average* lifetime in the bare bead is estimated to be 497 ns. The probes in the silver shells displayed a progressive decrease of lifetime with the shell growth that is shortened to nearly 140 ns at the shell thickness of 20 nm, about 1/4 that of the bare bead. The decay curves of R6G-labeled shells were analyzed by a single-exponential model and the data are listed in Table 4. The estimated lifetime in the bare bead is 4.14 ns. This value is shortened to 0.8 ns in the 30 nm shell, about 1/5 that of the bare bead. These results are probably due to an increase of the intrinsic decay rate in the shell.[4]

5. Brightness of Particles

For the Ru-labeled silver shells, the highest enhancement is 27 times when the bead contains the lowest concentration (20 μM) and is coated by 50 nm thick shell. However, the maximum efficiency may not correspond to the brightest probe due to the low content of fluorophore in it. By using free $Ru(bpy)_3^{2+}$ complex as reference, the brightness of shells with various concentrations was compared and plotted against the concentration (Figure 8). It is shown that the sample with 2×10^{-4} M of complex in the core with a 30 nm shell displays the highest brightness, which is 600 times brighter than a single molecule of free complex.

Conclusions

The Stöber method was employed to synthesize the silica beads with an average diameter of 100 nm. These beads were respectively labeled with $Ru(bpy)_3^{2+}$ and R6G by physical adsorption during particle formation. The silver shells were deposited on the beads layer-by-layer via a chemical reduction of silver nitrate by sodium citrate. The metal thickness ranged from 5 to 50 nm. The emission properties were studied on the basis of fluorophore concentration in the metal shells. It was observed that the Ru-labeled shells display a narrower emission band relative to that of the bare bead, but the R6G-labeled shell did not. The reason is uncertain, but is probably due to the already narrow emission spectrum of R6G. The emission intensity was altered with shell thickness and the enhancement efficiency was found to depend on fluorophore concentration, and showed metal-enhanced self-quenching between the fluorophores. Poisson statistics was employed to describe the distribution of self-quenching distance between the neighbor fluorophores, using the bare-labeled bead as the reference. For the Ru-labeled shells, the estimated self-quenching distance was increased from 6 to 16 nm when the metal shells were grown from 0 to 50 nm, almost independent of the complex concentration. Lifetime becomes shorter with the shell growth supporting our prediction that the enhancement occurred through an increase of the intrinsic decay rate. Because each shell contains more than one fluorophore, the shell with the highest enhanced efficiency may not be the brightest. The Ru-labeled shell with 200 μM complex in the core and 20 nm shell thickness is the brightest probe, about 600 times brighter than free $Ru(bpy)_3^{2+}$ in water. In future work, we intend to synthesize more beads labeled with several organic fluorophores to investigate the mechanism of fluorescence enhancement in the metal shells and optimize the conditions for the synthesis of bright shell probes. These labeled core–shell structures will provide considerable promise for a novel type of biomarker.

Acknowledgments

This research was supported by a grant from the NIH (HG-02655, EB-00682, and NCRR, RR-08119).

References and Notes

1. (a) Feldheim, DL.; Foss, CA. Metal Nanoparticles. Synthesis, Characterization and Applications. Marcel Dekker, Inc.; New York: 2002. (b) Kreibig, U.; Vollmer, M. Optical Properties of Metal Clusters. Springer-Verlag; Berlin and Heidelberg, Germany: 1995.
2. (a) Kamat PV. J. Phys. Chem. B 2002;106:7729. (b) Rosi NL, Mirkin CA. Chem. Rev 2005;105:1547. [PubMed: 15826019] (c) Love JC, Estroff LA, Kriebel JK, Nuzzo RG, Whitesides GM. Chem. Rev 2005;105:1103. [PubMed: 15826011]
3. Lakowicz, JR. Emerging biomedical application of time-resolved florescence spectroscopy. In: Lakowicz, JR., editor. Topics in Fluorescence spectroscopy. Vol. 4. Plenum Press; New York: 1994. Probe Design and Chemical Sensing
4. (a) Lakowicz JR. Anal. Biochem 2001;298:1. [PubMed: 11673890] (b) Lakowicz JR. Anal. Biochem 2005;337:171. [PubMed: 15691498]
5. (a) Sinner EK, Reuning U, Kok FN, Sacca B, Moroder L, Knoll W, Oesterhelt D. Anal. Biochem 2004;333:216. [PubMed: 15450795] (b) Bjerneld EJ, Foldes-Papp Z, Kall M, Rigler R. J. Phys. Chem. B 2002;106:1213. (c) Sokolov K, Chumanov G, Cotton TM. Anal. Chem 1998;70:3898. [PubMed: 9751028] (d) Kummerlen J, Leitner A, Brunner H, Aussenegg FR, Wokaun A. Mol. Phys 1993;80:1031.
6. (a) Millstone JE, Park S, Shuford KL, Qin L, Schatz GC, Mirkin CA. J. Am. Chem. Soc 2005;127:5312. [PubMed: 15826156] (b) Hubert C, Rumyantseva A, Lerondel G, Grand J, Kostcheev S, Billot L, Vial A, Bachelot R, Royer P, Chang S.-h. Gray SK, Wiederrecht GP, Schatz GC. Nano Lett 2005;5:615. [PubMed: 15826096] (c) Payne EK, Shuford KL, Park S, Schatz GC, Mirkin CA. J. Phys. Chem. B 2002;106:2150. (d) Evanoff DD, White RL, Chumanov G. J. Phys. Chem. B 2004;108:1522. (e) Kelly KL, Coronado E, Zhao LL, Schatz GC. J. Phys. Chem. B 2003;107:68.

7. (a) Messinger BJ, von Raben KU, Chang RK, Barber PW. Phys. Rev. B 1981;24:649. (b) Quinten M. Appl. Phys. B: Laser Opt 2001;73:245. (c) Kneipp K, Kneipp H, Itzkan I, Dasari DR, Feld MS. Chem. Rev 1999;99:2957. [PubMed: 11749507]
8. (a) Kumbhar AS, Kinnan MK, Chumanov G. J. Am. Chem. Soc 2005;127:12444. [PubMed: 16144364] (b) Bruzzone S, Malvaldi M, Arrighini GP, Guidotti C. J. Phys. Chem. B 2005;109:3807. [PubMed: 16851429]
9. (a) Jackson JB, Halas NJ. J. Phys. Chem. B 2001;105:2743. (b) Pham T, Jackson JB, Halas NJ, Lee TR. Langmuir 2002;18:4915. (c) Jiang, Z.-j.; Liu, C.-y. J. Phys. Chem. B 2003;107:12411. (d) Sun Y, Wiley B, Li Z-Y, Xia Y. J. Am. Chem. Soc 2004;126:9399–9406. [PubMed: 15281832]
10. (a) Hirsch LR, Jackson JB, Lee A, Halas NJ, West JL. Anal. Chem 2003;75:2377. [PubMed: 12918980] (b) Nehl CL, Grady NK, Goodrich GP, Tam F, Halas NJ, Hafner JH. Nano Lett 2004;4:2355. (c) Wang Y, Xie X, Wang X, Ku G, Gill KL, O'Neal DP, Stoica G, Wang LV. Nano Lett 2004;4:1689. (d) Alvarez-Puebla RA, Ross DJ, Nazri G-A, Aroca RF. Langmuir 2005;21:10504. [PubMed: 16262313]
11. (a) Limmer SJ, Chou TP, Cao G. J. Phys. Chem. B 2003;107:13313. (b) Sun Y, Wiley B, Li Z-Y, Xia Y. J. Am. Chem. Soc 2004;126:9399. [PubMed: 15281832] (c) Wang H, Tam F, Grady NK, Halas NJ. J. Phys. Chem. B 2005;109:18218. [PubMed: 16853342] (d) Radloff C, Vaia RA, Brunton J, Bouwer GT, Ward VK. Nano Lett 2005;5:1187. [PubMed: 15943466] (e) Shi W, Sahoo Y, Swihart MT, Prasad PN. Langmuir 2005;21:1610. [PubMed: 15697315] (f) K. E. Xu X, Bulcock SR, Cortie MB. J. Phys. Chem. B 2005;109:21516. [PubMed: 16853793]
12. Hao E, Li S, Bailey RC, Zou S, Schatz GC, Hupp JT. J. Phys. Chem. B 2004;108:1224.
13. Schelm S, Smith GB. J. Phys. Chem. B 2005;109:1689. [PubMed: 16851144]
14. (a) Zhang J, Gryczynski I, Gryczynski Z, Lakowicz JR. J. Phys. Chem. B 2006;110:8986. [PubMed: 16671705] (b) Zhang J, Fu Y, Lakowicz JR. J. Phys. Chem. C 2007;111:50.
15. Sabatani E, Nikol HD, Gray HB, Anson FC. J. Am. Chem. Soc 1996;118:1158.
16. (a) del Monte F, Mackenzie JD, Levy D. Langmuir 2000;16:7377. (b) Ferrer ML, del Monte F, Levy D. Langmuir 2003;19:2782.
17. Stober W, Fink A, Bohn E. J. Colloid Interface Sci 1968;26:62.
18. (a) Wheeler J, Thomas JK. J. Phys. Chem 1982;86:4540. (b) Innocenzi P, Kozuka H, Yoko T. J. Phys. Chem. B 1997;101:2285. (c) Matsui K, Sasaki K, Takahashi N. Langmuir 1991;7:2866.
19. (a) Whitten DG. Acc. Chem. Res 1993;26:502. (b) Whitten DG, Chen L, Geiger HC, Perlstein J, Song X. J. Phys. Chem. B 1998;102:10098.
20. Ogawa M, Nakamura T, Mori J.-i. Kuroda K. J. Phys. Chem. B 2000;104:8554.
21. (a) Enderlein J. Phys. Chem. Chem. Phys 2004;4:2780. (b) Enderlein J. Appl. Phys. Lett 2002;80:315.
22. (a) Gryczynski I, Malicka J, Gryczynski Z, Lakowicz JR. Anal. Biochem 2004;324:170. [PubMed: 14690680] (b) Lakowicz JR. Anal. Biochem 2004;324:153. [PubMed: 14690679]
23. (a) Yagi M, Nagai K, Onikubo T, Kaneko M. J. Electroanal. Chem 1995;383:61. (b) Nagai K, Takamiya N, Kaneko M. J. Photochem. Photobiol 1994;84:271.
24. Lakowicz, JR. Principles of Fluorescence Spectroscopy. Vol. 2nd ed.. Kluwer Academic; New York: 1999.

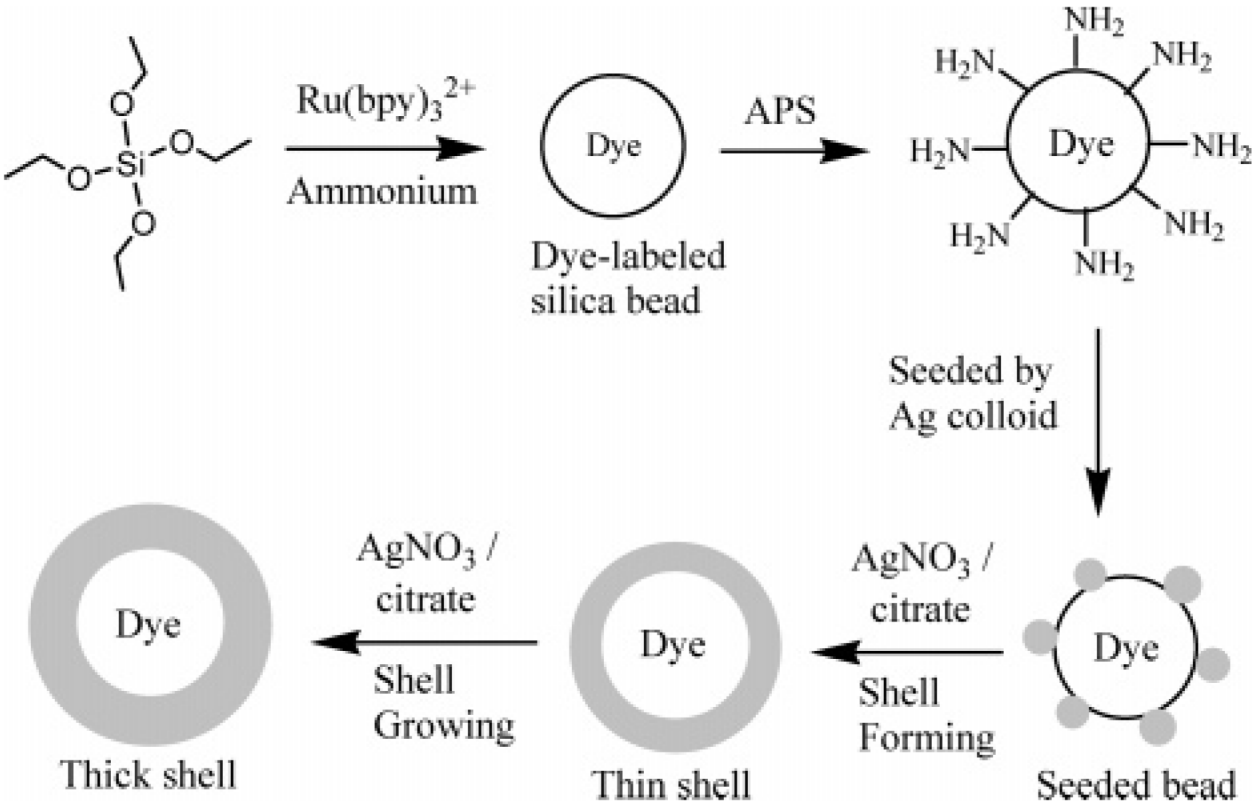

SCHEME 1.
Preparation of Ru-Labeled Silica Bead and Silver Nanoshell in a Particle-Seeding and Then Layer-by-Layer Growth Model

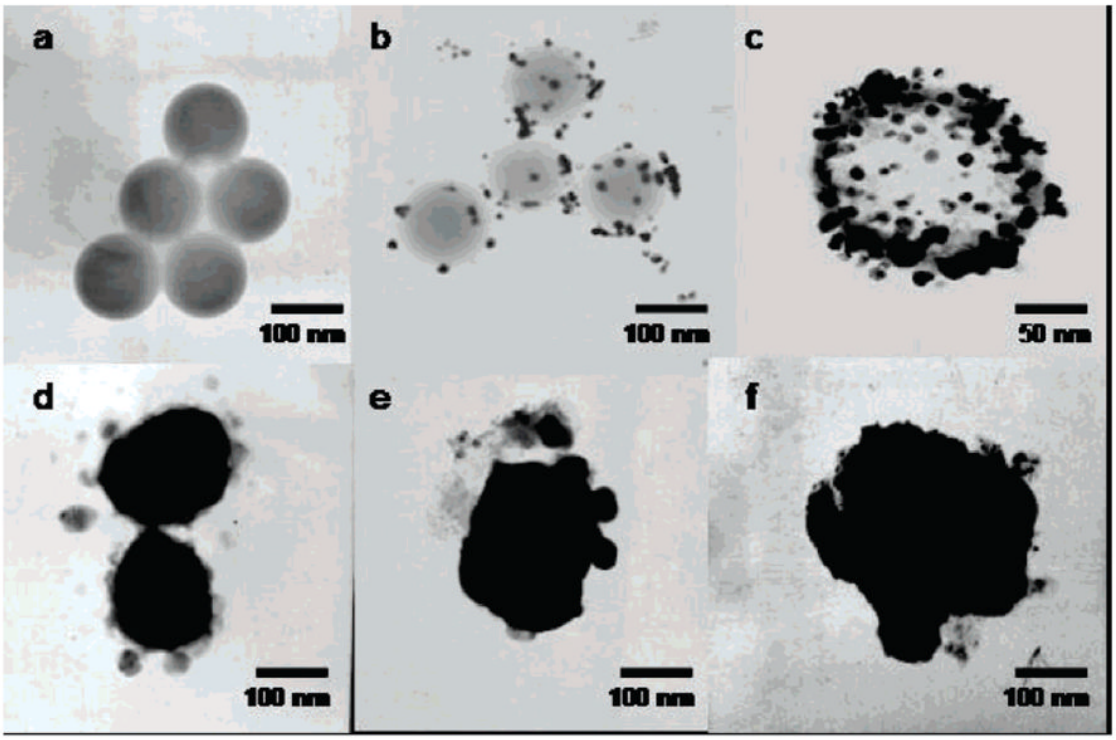

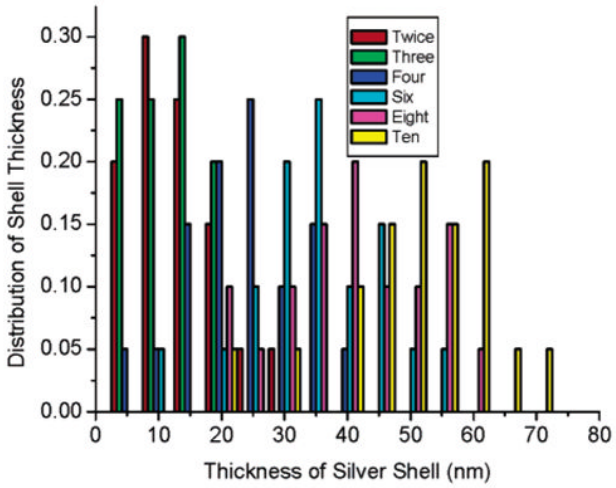

(g)

Figure 1.

TEM images for (a) silica beads with 100 nm diameter, (b) silica beads seeded by silver colloids, (c) silver shells with one coating (silver islands on silica beads), (d) silver shells with two coatings (10 nm metal shell), (e) silver shells with six coatings (30 nm metal shell), (d) silver shells with ten coatings (50 nm metal shell), and (g) distribution of silver shell thickness with the times of shell coating.

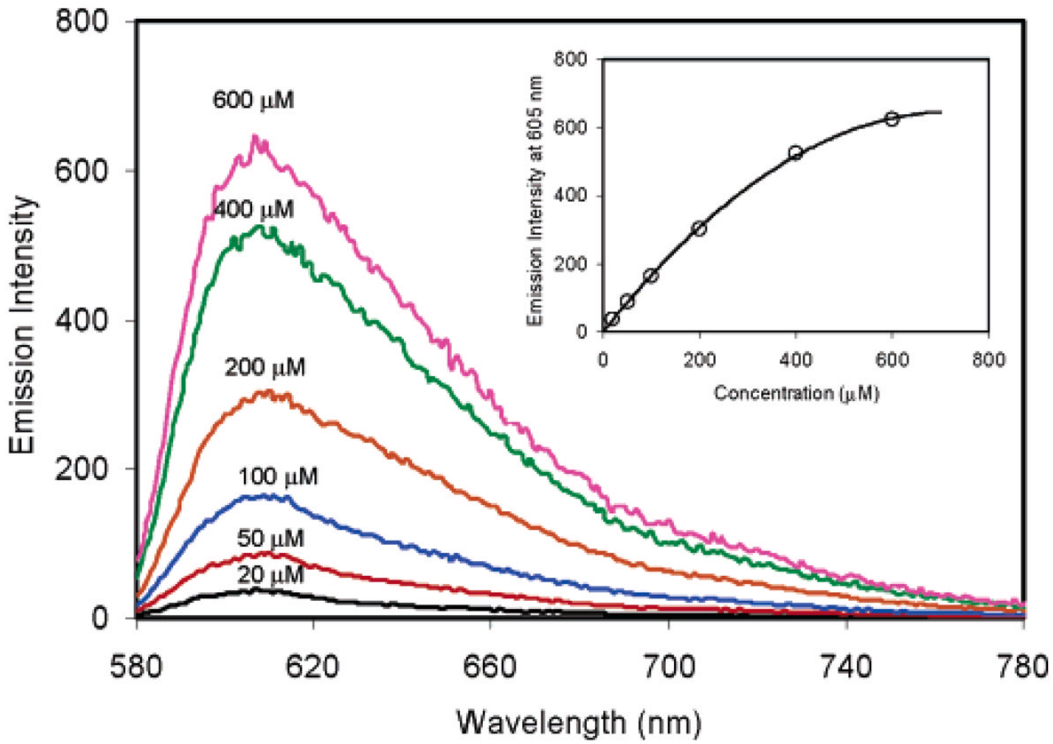

Figure 2.

Emission spectra of silica beads (10 nM) with different concentrations of $Ru(bpy)_3^{2+}$ complex upon excitation at 450 nm. The inset represents the dependence of emission intensity at 605 nm on the concentration of complex in the bare bead.

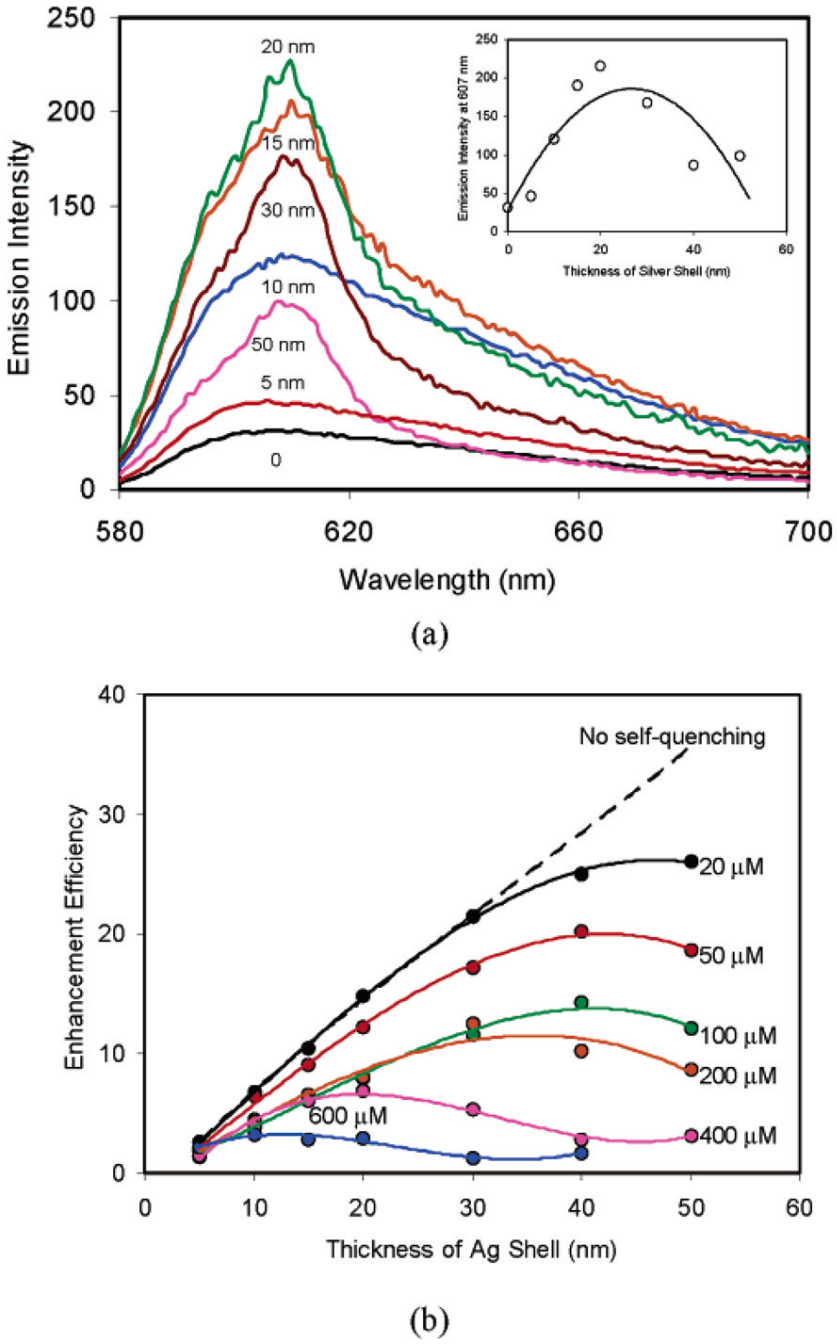

Figure 3.

(a) Emission spectra of 4×10^{-4} M Ru-labeled silica beads and their silver nanoshells with different thicknesses of metal shells upon excitation at 450 nm. The inset represents the dependence of the emission intensity at 605 nm on the shell thickness. (b) Dependence of the enhancement efficiency on the shell thickness.

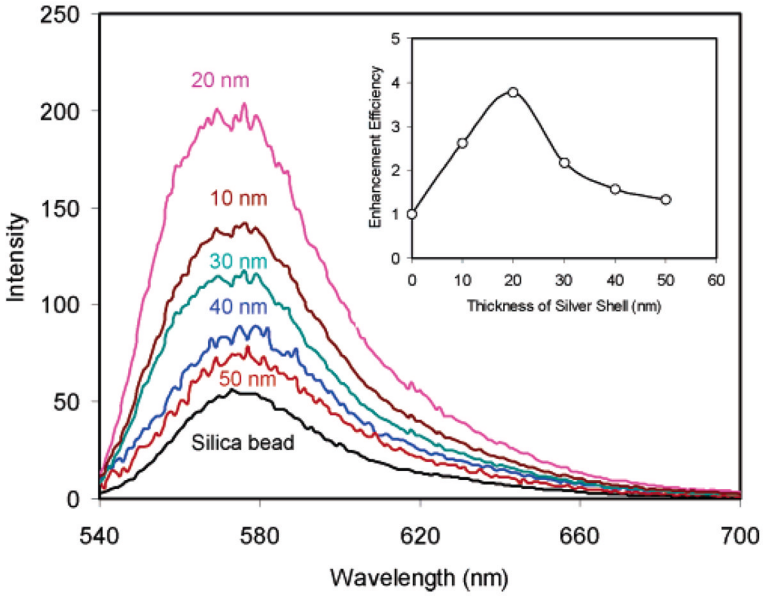

Figure 4.

Emission spectra of 2×10^{-4} M R6G-labeled silica beads and their silver nanoshells with different thicknesses of metal shells upon excitation at 450 nm. The inset represents the dependence of the emission intensity at 605 nm on the shell thickness.

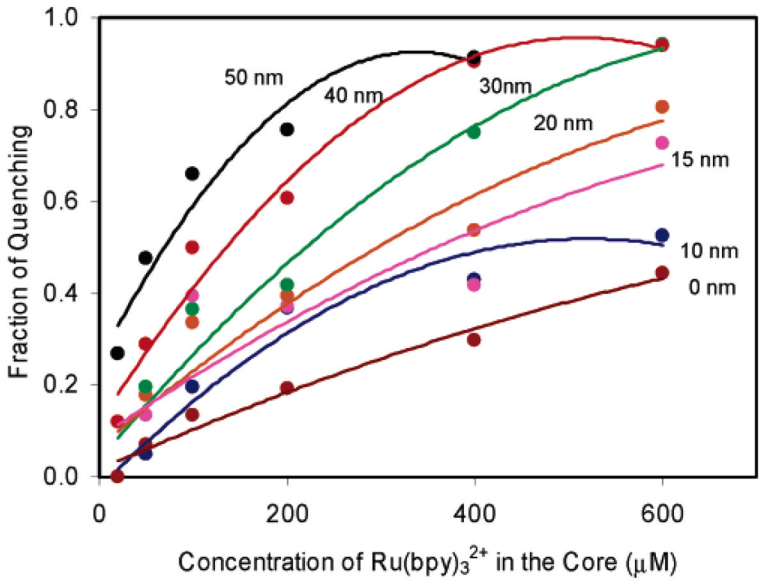

Figure 5.
Dependence of the quenching fraction on the local concentration in the core at different metal thicknesses for the Ru-labeled shell.

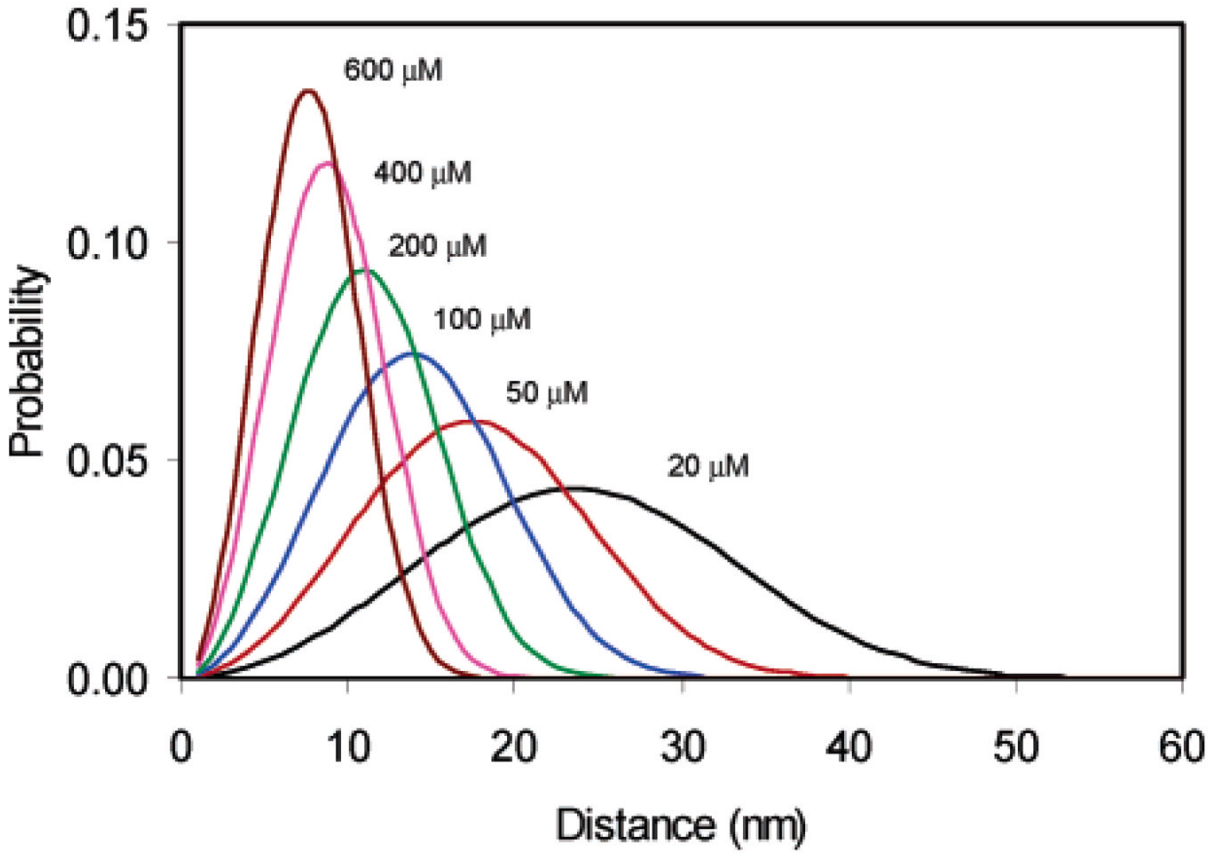

Figure 6.
Poisson distributions of the distance between the neighbor complexes in the silica beads with the different concentrations.

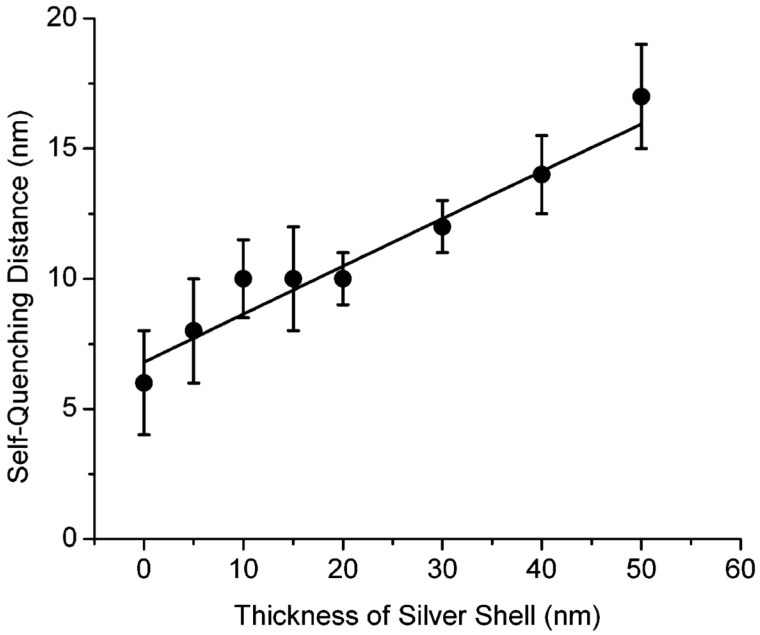

Figure 7.
Dependence of self-quenching distance on the shell thickness.

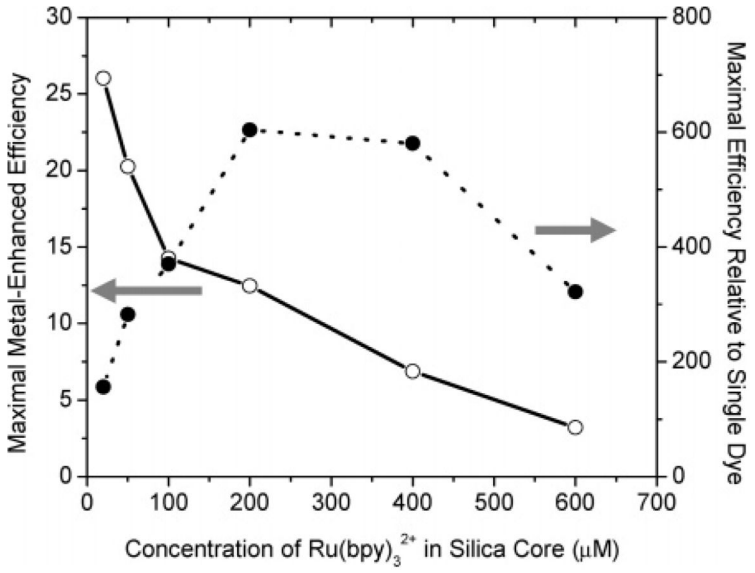

Figure 8.
Dependence of the maximal enhancement efficiency and emission efficiency on the thickness of the silver shell.

TABLE 1

Concentrations of the $Ru(bpy)_3^{2+}$ Complex in the Silica Beads and the Estimated Number of Complexes in Each Corresponding Bead When Prepared at Different Concentrations

concn of $Ru(bpy)_3^{2+}$ in soln (μM)	0.20	0.50	1.0	2.0	5.0	10
concn of $Ru(bpy)_3^{2+}$ in silica bead (μM)	2×10^1	5×10^1	1×10^2	2×10^2	4×10^2	6×10^2
av dye no. per bead	6	15	30	60	120	180

J Phys Chem C Nanomater Interfaces. Author manuscript; available in PMC 2009 October 19.

TABLE 2

Poisson Estimated Distance of Self-Quenching between Neighbor $Ru(bpy)_3^{2+}$ in the Silica Beads Containing Different Complex Concentrations and Coating with Different Thicknesses of Silver Shell

	distances[b] at different shell thicknesses[c] =							
concentration[a]	0	5	10	15	20	30	40	50
2×10^1							14	16
5×10^1		6	10	10	10	12	14	17
1×10^2	8	6	9	13	11	12	14	17
2×10^2	8	10	8	9	9	10	12	14
4×10^2	6	8	8	8	9	10	12	14
6×10^2	4	7	8	9	10	11	12	15

[a] Concentration of $Ru(bpy)_3^{2+}$ complex in silica core (μM).

[b] Self-quenching distance estimated from Poisson distribution curves in Figure 8.

[c] Silver shell thickness (nm).

TABLE 3

Lifetime Data for Ru-Labeled Silica Bead ($1 \times 10^2\ \mu$M) and Its Silver Shell.

samples	τ_i (ns)	α_i	$\langle\tau\rangle$ (ns)	χ_R^2
$1 \times 10^2\ \mu$M $Ru(bpy)_3^{2+}$ in bare bead	49.2	0.647	497.3	1.2
	568.4	0.353		
10 nm silver shell	41.1	0.762	161.9	1.4
	230.9	0.238		
20 nm silver shell	34.1	0.772	139.9	1.4
	200.8	0.228		
30 nm silver shell	33.0	0.800	141.4	0.9
	209.7	0.200		
40 nm silver shell	33.3	0.787	136.7	1.5
	200.02	0.213		
50 nm silver shell	32.6	0.799	139.8	1.3
	206.9	0.201		

TABLE 4

Lifetime Data for R6G-Labeled Silica Bead and Its Silver Shells

samples	τ_i (ns)	χ_R^2
2×10^2 μM R6G in bare bead	4.14	1.1
10 nm silver shell	2.81	1.4
20 nm silver shell	0.88	1.2
30 nm silver shell	0.82	1.3
40 nm silver shell	0.96	1.4
50 nm silver shell	1.02	1.3